Journal of Electron Spectroscopy and Related Phenomena xxx (xxxx) xxx–xxx

Contents lists available at ScienceDirect

Journal of Electron Spectroscopy and Related Phenomena

journal homepage: www.elsevier.com/locate/elspec

# Optical and electronic properties of amorphous silicon dioxide by single and double electron spectroscopy

Vytautas Astašauskas[a,*], Alessandra Bellissimo[b], Pavel Kuksa[a], Christian Tomastik[a], Henryk Kalbe[a], Wolfgang S.M. Werner[a]

[a] Institut für Angewandte Physik, Vienna University of Technology, Wiedner Hauptstrasse 8-10, 1040 Vienna, Austria
[b] Dipartimento di Scienze, Università degli Studi Roma Tre, Via della Vasca Navale 84, 00146 Rome, Italy

A B S T R A C T

An investigation of the optical and electronic properties of amorphous silicon dioxide by means of a combination of reflection electron energy loss spectroscopy (REELS) and secondary electron–electron energy loss coincidence spectroscopy (SE2ELCS) is presented. Optical constants for a-$SiO_2$ were extracted from the REELS measurements and a band gap of 9.1 eV was determined by deconvolution of multiple scattering and fitting the differential inverse inelastic mean free path with a model energy loss function (ELF). The coincidence measurements allow to determine the surface barrier height and the electron affinity was determined to be 0.8 eV. Furthermore, the coincidence measurements show that even in the case of an insulator, plasmon decay is the main mechanism for generation of secondary electrons.

## 1. Introduction

Insulators constitute a class of materials of special interest regarding particle induced electron emission, in particular electron induced emission of slow electrons [1]. Owing to their high yield for secondary electron emission such materials play an important role in e.g. particle detection [2,3] and plasma display devices [4,5]. The interaction of low energy electrons with insulating materials is also of great technological and fundamental importance in the case of photoresist materials in electron beam lithography since it is responsible for the proximity effect or biomaterials such as DNA for studies connected with radiation damage.

The interaction of low energy electrons with such materials as well as the emission of secondary electrons from insulators is special in two respects, both connected with their electronic structure: (1) due to the presence of a band gap in insulators, or, in other words, the absence of unoccupied states above the valence band maximum, electrons with energies smaller than the band gap cannot induce an inelastic process in an ideal defect-free insulator. In consequence, the mean free path for inelastic electron scattering is very high compared to that of e.g. a metal, particularly at low energies of special importance for the secondary electron cascade; and (2) the escape over the surface barrier is commonly assumed to be governed by the electron affinity $\chi$, rather than the inner potential $U_i$, as in the case of a metal. Both of the above effects lead to large values of the secondary electron yield (SEY) for insulators, i.e. the number of emitted electrons per incident primary electron.

In the present work, a method is described to determine the above parameters for a non-crystalline insulator by using single and double electron spectroscopy. It is shown that the electron affinity $\chi$, energy band gap $E_g$, height of the surface barrier $U_i$, optical constants and the inelastic mean free path (IMFP) can be retrieved in-situ, by using the same equipment for all measurements and without breaking the vacuum. Since electrons are used as the probing particles, the method is very surface sensitive and therefore is ideal to distinguish the influence of surface defects. To eliminate multiple (or plural) scattering from the raw data, deconvolution algorithms are employed to achieve a clear separation of surface and bulk scattering and to determine the bulk optical properties as well as the electron inelastic mean free path.

The mechanism of secondary electron production in $SiO_2$ is investigated by means of the double differential coincidence yield. It is found that this proceeds via the incoherent excitation and decay of (multiple) plasmons each of which decays into a single secondary electron.

Amorphous $SiO_2$ was chosen as an example of application since $SiO_2$ is an extremely important material in microelectronics, and is used in the vast majority of semiconductor devices as the gate dielectric. Silicon dioxide is also widely used in glass, ceramics industry, optical fibers. In particular, the presence of defects in $SiO_2$ is important for metal-oxide-semiconductor (MOS) devices since they can cause a dielectric breakdown. Such defects can be identified rather trivially by using the methodology described in the following sections.

* Corresponding author.
*E-mail address:* astasauskas@iap.tuwien.ac.at (V. Astašauskas).

https://doi.org/10.1016/j.elspec.2019.02.008
Received 5 October 2018; Received in revised form 18 January 2019; Accepted 12 February 2019

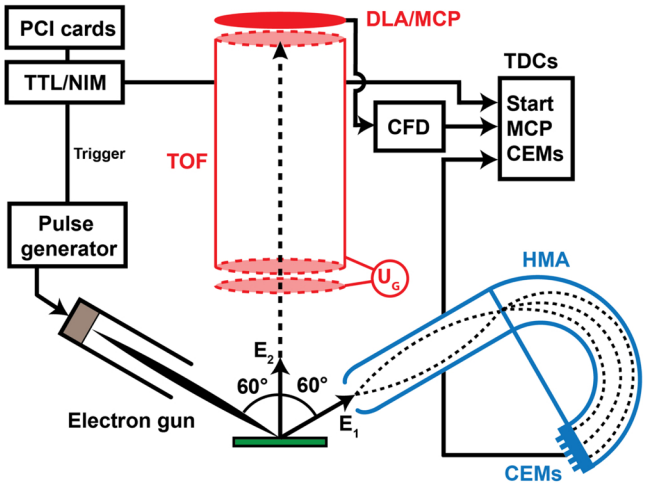


**Fig. 1.** Schematic view of the SE2ELCS spectrometer.

## 2. Experiment

The sample was a 100 nm thick amorphous silicon dioxide film thermally grown on an amorphous Si-substrate. Reflection electron energy loss (REELS) measurements were performed using a Thermofisher Microlab 310F instrument. The REELS measurements were made in two different kinematic conditions: one more bulk sensitive, with the sample being in the flat position (incidence angle 0°, detection angle 60° with respect to the surface normal) at 3000 eV incident energy and the second more surface sensitive where the sample was tilted by 20° (incidence angle 20°, detection angle 80° w.r.t. the surface normal), at 500 eV incident energy. Further experimental details can be found in references [6] and [7]. Electron-electron coincidence measurements were performed using the SE2ELCS (secondary electron–electron energy loss coincidence spectroscopy) spectrometer at the Vienna University of Technology. The schematic view and the geometrical configuration of the SE2ELCS spectrometer are given in Fig. 1. The sample is irradiated with a continuous beam of electrons at very low currents (in the sub-pA range) and having the energy spread of 0.6 eV. Note that the plane of incidence and the plane of detection enclose an angle of 35° at an incidence angle of 60° with respect to the surface normal. After the interaction with the surface, back reflected electrons are detected with the hemispherical mirror analyzer (HMA). The axis of the entrance lens describes an angle of 60° with the surface normal. As the second detector, a time-of-flight (TOF) analyzer is used, which due to its' sensitivity at low energies is used to collect the secondary electrons coming out of the sample. The TOF analyzer consists of a drift tube and the detector is a stack of two multi-channel-plates (MCP) and a hexagonal delay line anode (DLA). During the measurement the TOF analyzer records all events with a time resolution of about 60 ps, while the energy observed by the HMA is scanned from the incident energy down to several eV. The overall tim resolution of the coincidence measurements is of the order of a few nanoseconds, determined by the flight time spread of the scattered electrons in the HMA. During a separate calibration measurement, an arrival time spectrum in the HMA is recorded using a pulsed electron beam. In this way, the flight time of electrons from the sample to the channeltrons is determined for each energy used in the coincidence measurements. Using such calibration measurements allows one to operate a coincidence measurement with a continuous beam, in this way increasing the coincidence count rate considerably. The gain in performance can be estimated on the basis of Poisson distribution. Assuming that 0.1 electrons per pulse sufficiently reduce the probability for electron pairs to be emitted in the primary pulse, the gain is almost a factor of 100. In the case of the coincidence measurements, the pass energy of the HMA is set to 200 eV, maximizing the transmission and leading to the energy resolution of 5 eV. All measurements are performed in ultra high vacuum, maintaining a pressure of $2 \cdot 10^{-10}$ mbar over the whole measurement duration (typically several weeks for the coincidence measurements).

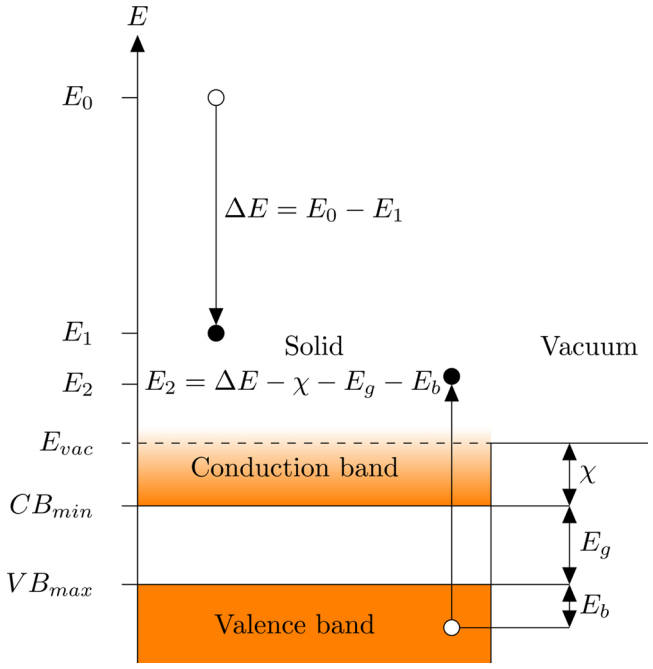


**Fig. 2.** Energy diagram of an insulator. $\chi$ – electron affinity, $E_g$ – band gap. An electron, having received $\Delta E$ energy through an inelastic collision is liberated from the solid with $E_2$ being the kinetic energy outside the solid. Note that in the following the binding energy $E_b$ is counted from the top of the valence band.

## 3. Determination of the band gap and electron affinity

The method used in this work to determine the electronic structure parameters, relies on the fact that different energy levels are probed by a (singles) reflection electron energy loss measurement compared with a coincidence measurement [8] (see Fig. 2). In the case of an insulator, the conduction band is separated from the valence band by the energy gap $E_g$. Since the least bound electron resides in the top of the valence band in the solid, the lowest energy needed for it to leave the solid is equal to the height of the surface barrier $U_i = \chi + E_g$ (provided that the bottom of the conduction band is below the vacuum level, i.e. for a positive electron affinity). In the above, $\chi$ is the electron affinity or the energy difference between the bottom of the conduction band and the vacuum level. Since in an undoped, defect-free insulator there are no possible electron states in the band gap $E_g$, the lowest energy loss possible is equal to the band gap, which is represented by the promotion of an electron from the top of the valence band to the bottom of the conduction band. This scenario can be seen by conducting a Reflection Electron Energy Loss measurement which is often used to determine the band gap of insulators [9,10]. However, this is only valid if the material is perfectly clean, has no defects or dopants. Otherwise, additional states may appear in the band gap and transitions with lower energies become possible. In contrast, in the (e,2e)-coincidence experiment two electrons are always detected. In other words, only if the slow electron liberated by an energy loss of the fast electron is also detected, a coincidence count (i.e. detection of an electron pair) is recorded. From the schematic energy diagram in Fig. 2 the energy balance in an (e,2e) coincidence experiment is described by:

$$E_b = E_0 - (E_1 + E_2) - (\chi + E_g) \quad (1)$$

where $E_0$ is the energy of the incoming electron. Note that Eq. (1)

implies that the energy sum $E_1 + E_2$ of an electron pair in an (e,2e) coincidence spectrum determines the binding energy scale of the bound solid state electron before ejection.

The lowest energy loss for which coincidences start to appear is determined by the minimum energy $\Delta E$ sufficient for the emission of the second electron with zero binding energy, which is then emitted with an energy $E_2$ above the vacuum level:

$$E_2 = \Delta E_{\min} - \chi - E_g \simeq 0 \tag{2}$$

Therefore the lowest energy loss recorded in the coincidence experiment is determined by the height of the surface barrier ($U_i = \Delta E_{min}$) rather than the band gap and the electron affinity can be retrieved from:

$$\chi = U_i - E_g = \Delta E_{\min} - E_g \tag{3}$$

## 4. Determination of optical constants

The susceptibility of the solid to become polarized by an external perturbation is described by the dielectric function $\epsilon(\omega, q)$ where $\hbar\omega$ and $\hbar q$ denote the energy and momentum transfer in an inelastic collision. In the following we use atomic units $\hbar = e = 1$. This quantity can be retrieved by energy loss measurements, since they sample the energy loss function (ELF) $\mathrm{Im}(-1/\epsilon)$ of the solid. However, REELS is dominated by multiple scattering, which needs to be eliminated from experimental data. Furthermore, the measured spectra always contain both bulk (infinite medium) and surface scattering (taking place at the vacuum-solid boundary), therefore it is also necessary to properly distinguish bulk and surface contributions. This is done by measuring two loss spectra $y_1(E)$ and $y_2(E)$ under different kinematic conditions such that the relative importance of surface and bulk scattering is significantly different in the two spectra. Since the probability for surface excitations depends on the electron energy $E$ and the polar surface crossing angle $\theta$ as [11]:

$$P_s \propto \frac{1}{\sqrt{E}\cos\theta}, \tag{4}$$

this can be achieved by choosing appropriate energies and/or geometrical configurations. The method described in Ref. [12] then consists of first eliminating multiple scattering using the Tougaard–Chorkendorff deconvolution algorithm [13]:

$$y^*_{1,2}(T) = y_{1,2}(T) - \int_0^T y_{1,2}(T - T')y_1^*(T')\mathrm{dT}' \tag{5}$$

The resulting spectra $y_1^*(T)$ and $y_2^*(T)$ are so called "effective" cross sections for inelastic scattering for energy loss $T$. The single scattering loss distributions can then be derived by using the bivariate reversal method [11] yielding for the single scattering distributions:

$$w(T) = u_{10}y_1^*(T) + u_{01}y_2^*(T) + u_{11}y_1^* \otimes y_2^*(T) \tag{6}$$

where $u_{ij}$ are coefficients which are different for bulk and surface components. Further details can be found in Ref. [11].

The upper panel in Fig. 3 shows the REELS measured with 500 eV (red curve, more surface sensitive) and 3000 eV primary energy (blue curve, more bulk sensitive). A Lucy–Richardson deconvolution algorithm [14] was applied to both spectra to eliminate the instrumental broadening of the elastic peak. The elastic peaks of the spectra have been removed and the intensity normalized by its area. Both spectra exhibit characteristic plasmon peaks at around 22 eV energy loss and the double plasmon losses at 40–45 eV loss. At lower energy losses, several peaks/shoulders can be seen, especially in the surface-sensitive spectrum, however the locations of the peaks are difficult to determine.

The bottom panel in Fig. 3 shows the loss spectra after deconvolution of multiple scattering by the Tougaard–Chorkendorff (TC) deconvolution algorithm [13], as evidenced by the significant decrease of intensity above 25 eV (the multiple scattering region of the spectrum).

Fig. 4 shows the result after applying the bivariate reversal

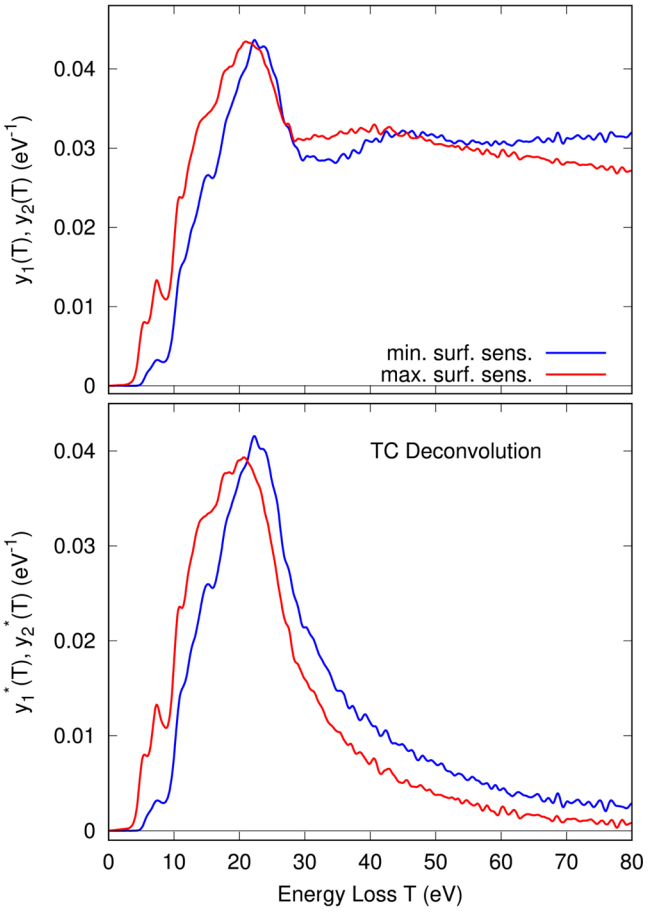


**Fig. 3.** Upper panel: energy loss spectra, in absolute units, after the subtraction of the elastic peak and normalization to the area of the elastic peak; lower panel: energy loss spectra after TC-deconvolution to eliminate multiple scattering.

algorithm to separate bulk scattering from surface scattering. The top panel shows the differential surface excitation probability (DSEP), or the distribution of energy losses in a single surface crossing, in comparison with the surface loss function

$$\mathrm{Im}\frac{(\epsilon - 1)^2}{\epsilon(\epsilon + 1)} = 4\mathrm{Im}\frac{-1}{1 + \epsilon} - \mathrm{Im}\left(\frac{-1}{\epsilon}\right), \tag{7}$$

where data for $\epsilon(\omega, q)$ were taken from Palik's book [15]: The second term in Eq. (7) describes the bulk part of surface excitations and is commonly referred to as the Begrenzung's effect, due to which the intensity of bulk excitations is suppressed in the vicinity of the surface. This is seen as the negative excursion of the surface loss function in the upper panel of Fig. 4.

It can be immediately seen in the DSEP spectrum that the loss features between 5 and 20 eV energy loss are more pronounced and their energies can be easily determined, in contrast to the loss spectra before and after TC deconvolution (Fig. 3).

The energies of these features have been determined and are given in Table 1. There is a good agreement of the position of the energy loss peaks with Palik's data with the exception of the two peaks G1 and G2 at an energy loss of 5.3 eV and 7.3 eV. Such losses have been observed before and have been attributed to oxygen-related defects [16], due to which additional states in the bandgap appear [17]. The sharp peak at 10.6 eV energy loss (denoted "E") is commonly known as an excitonic peak. However, in Ref. [18] it was argued that this peak has partly interband character. The next three peaks T1, T2 and T3 at 12.3 eV, 13.6 eV and 17.3 eV respectively were attributed to interband transitions [19]. The bottom panel of Fig. 4 shows the differential inelastic

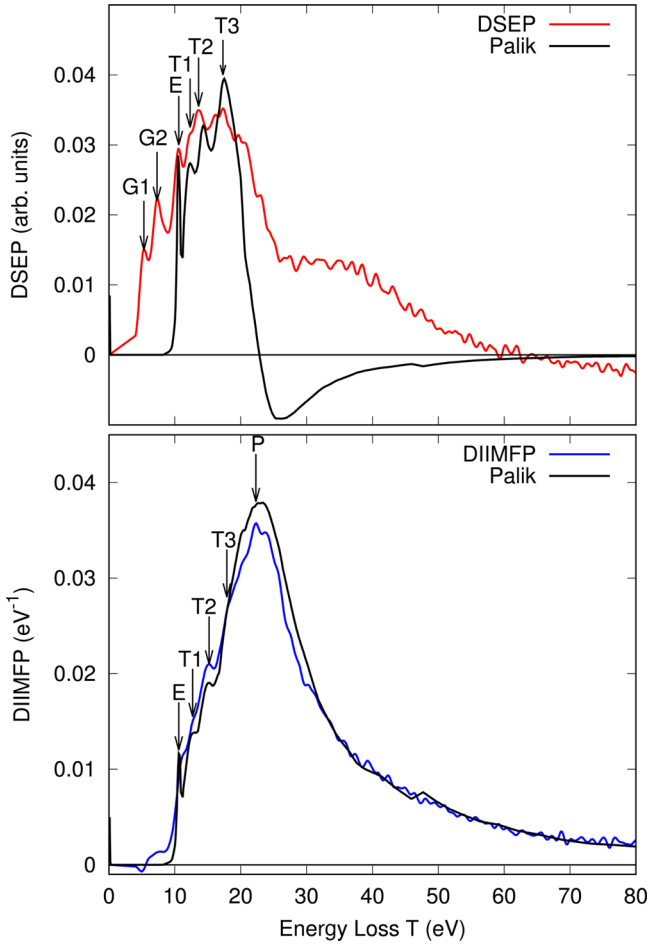


**Fig. 4.** Upper panel: differential surface excitation probability compared with the scaled surface loss function; Lower panel: normalized differential inelastic inverse mean free path on an absolute scale compared with the scaled energy loss function according to Palik's book [15]. G(1,2) – band gap states, E – exciton, T(1,2,3) – interband transitions, P – plasmonic excitation.

**Table 1**
Energies of loss features in the DIIMFP and DSEP.

| Loss feature | Bulk (eV) | Surface (eV) |
|---|---|---|
| G1 | – | 5.3 |
| G2 | – | 7.3 |
| E | 10.6 | 10.6 |
| T1 | 12.7 | 12.3 |
| T2 | 15.2 | 13.6 |
| T3 | 17.9 | 17.3 |
| P | 22.3 | – |

inverse mean free path $W_b$, which describes the probability of a specific energy loss event for all momentum transfers. It can be calculated by:

$$W_b(\omega) = \frac{1}{\pi E_0}\int_{q_-}^{q_+}\frac{1}{q}\mathrm{Im}\left[\frac{-1}{\epsilon(\omega, q)}\right]\mathrm{d}q \tag{8}$$

where $q_\pm = \sqrt{E} \pm \sqrt{E-\hbar\omega}$. In the case of insulators with flat bands plasmon dispersion is assumed to be weak, which makes it possible to directly compare the resulting DIIMFP with the energy loss function (ELF) $\mathrm{Im}(-1/\epsilon(\omega, q))$ (e.g. the one reported in by Palik) after scaling.

It is evident that the shape of the DIIMFP is much different from the DSEP and the band gap states G1 and G2 are no longer visible in the bulk. Such result confirms the hypothesis that such states are caused by defects near the surface. As in the case of the DSEP also the DIIMFP contains the excitonic level (even though less intense) and the three interband transitions with slight shifts of 0.4–1.6 eV. The maximum of the DIIMFP corresponds to the plasmon excitation at 22.3 eV as observed by other authors [18,19].

It has to be noted that just by using the loss spectra or TC-deconvoluted data it is very difficult to determine the energy or location (surface or bulk) of transitions occurring in the solid. However, the bivariate reversal method used here is able to extract this information.

The DIIMFP was fitted by using the Drude–Lindhardt model [20,21] which describes the dielectric function by a set of oscillators having amplitudes $A_i$, binding energies $\omega_i$ and damping parameters $\Gamma_i$:

$$\epsilon_1(\omega, q) = \epsilon_b - \sum_i \frac{A_i(\omega^2-\omega_i^2)}{(\omega^2-\omega_i^2)^2+\Gamma_i^2\omega^2} \tag{9}$$

$$\epsilon_2(\omega, q) = \sum_i \frac{A_i\Gamma_i\omega}{(\omega^2-\omega_i^2)^2+\Gamma_i^2\omega^2} \tag{10}$$

where $\epsilon_1$ is the real (dispersive part) and $\epsilon_2$ is the imaginary (absorptive) part of the dielectric function. Flat bands were assumed, i.e. no dispersion of the resonance frequencies $\omega_i(q) = \omega_i(0)$. The experimentally determined DIIMFP was fitted with the model dielectric function by using Eqs. (8)–(10) and minimizing the $\chi$-square difference between the model and experiment with a nonlinear optimisation algorithm [22]. The determined fit parameters $A_i$, $\Gamma_i$ and $\omega_i$ are given in Table 2 and the resulting fit is shown in Fig. 5.

Note that the model summarized by Eqs. (9) and (10) merely serves as a mathematical interpolation of the experimental data in Fig. 5. Care should be taken when attempting to associate any physical process with the values of the retrieved parameters.

The inelastic mean free path (IMFP) λ has been determined by using the Penn [23] and Mermin [24] models and integration of the DIIMFP. The results are given in Fig. 6 where it is compared with the values estimated by the TPP-2M formula [25]. The determined IMFP values agree reasonably well with the TPP-2M formula, with a maximum deviation of around 10 percent.

## 5. (e,2e) coincidence measurements of plasmon decay in $SiO_2$

The results of the coincidence measurements are given in Fig. 7. The colorscale of Fig. 7b represents the intensity of correlated electron pairs consisting of two electrons that have interacted with each other. During the inelastic interaction, part of the incident energy is transferred to solid state electrons. If this energy transfer to the secondary electron is sufficient to overcome the potential barrier, it can be liberated from the solid. Thus each electron pair consists of the scattered electron (having energy $E_1$) and the emitted secondary electron (having energy $E_2$). Note that the $E_1$ scale is uniform while the $E_2$ scale is converted from flight times – therefore the energy resolution deteriorates quickly above 20 eV. It has been shown in Fig. 2 that a constant binding energy corresponds to a diagonal line on which $E_1 + E_2 = const.$ The red line in Fig. 7 corresponds to zero binding energy, while the green dashed line indicates the sum energy being equal to the incident energy.

The comparison of the singles electron energy loss spectrum of $SiO_2$ with the single and double differential spectra (w.r.t. energy loss in Fig. 7a and energy loss and energy $E_2$ of the second electron in Fig. 7b) clearly illustrates the important role of the plasmon in the context of the

**Table 2**
Optical constants of $SiO_2$ as fit parameters for Eqs. (9) and (10).

| $A_i$ (eV$^2$) | $\Gamma_i$ (eV) | $\omega_i$ (eV) |
|---|---|---|
| 235.66 | 4.7 | 14.3 |
| 3250.99 | 11.2 | 21.2 |
| 589.27 | 5.9 | 24.4 |
| 967.66 | 12.1 | 31.7 |
| 1659.71 | 23.4 | 43.9 |
| 41723.28 | 446.4 | 117.0 |

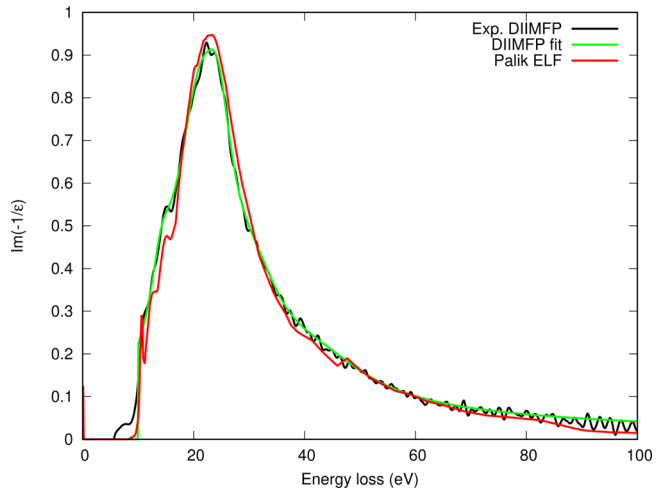


**Fig. 5.** Fit of the experimentally determined DIIMFP (green solid line, scaled), compared with the energy loss function by Palik [15].

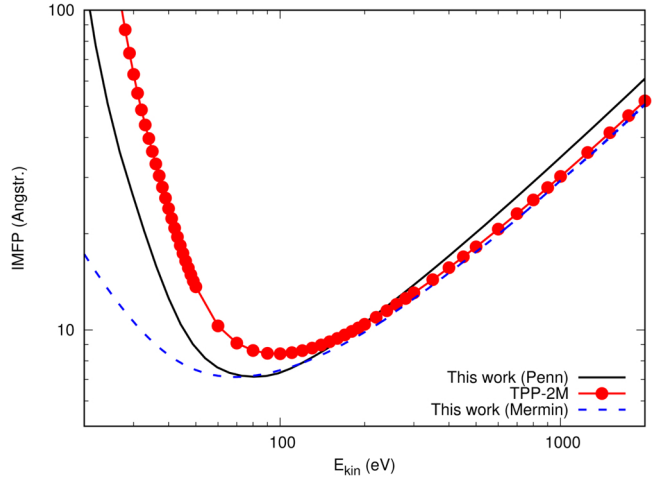


**Fig. 6.** Inelastic mean free path (IMFP) of $SiO_2$ according to Penn model [23] (dotted line) and according to Mermin [24] (dashed line) compared with the results of the TPP-2M formula [25].

elementary excitations of the solid state electrons. As discussed above in the context of Figs. 3–5, the intensity in the loss spectra for energy losses $\Delta E < 30$ eV is almost entirely made up by surface and bulk plasmon excitation. The existence of the plasmon (even in the case of an insulator) is evidenced by the zero in the real part of the dielectric function at $\omega_p = 22.3$eV for the oscillators specified in Table 2 and describes a short-lived (the plasmon peak has quite a substantial width) collective oscillation of a number of solid state electrons (of the order of 10), in accordance with the "momentum exciton"-model proposed by Ferrell [26], i.e. a coherent superposition of a number of electron-hole pairs which together constitute the plasmon.

While the analysis of the singles electron energy loss spectrum clearly demonstrates the existence of the plasmon as the main elementary excitation in $SiO_2$, the results of the coincidence measurements presented in Fig. 7 allow some conclusions to be made concerning its decay: in the range of energy losses $\Delta E < 30\,eV$, mainly corresponding to single inelastic scattering events, the main intensity in the double differential data in Fig. 7b is provided by a feature parallel to the red line, corresponding to emission of solid state electrons from near the valence band maximum (see Fig. 2 and Eq. (1)). The range of binding energies involved in this single scattering feature the emission is seen to be approximately 4 eV, being of the order of the width of the first valence band. This implies that the energy loss experienced by the

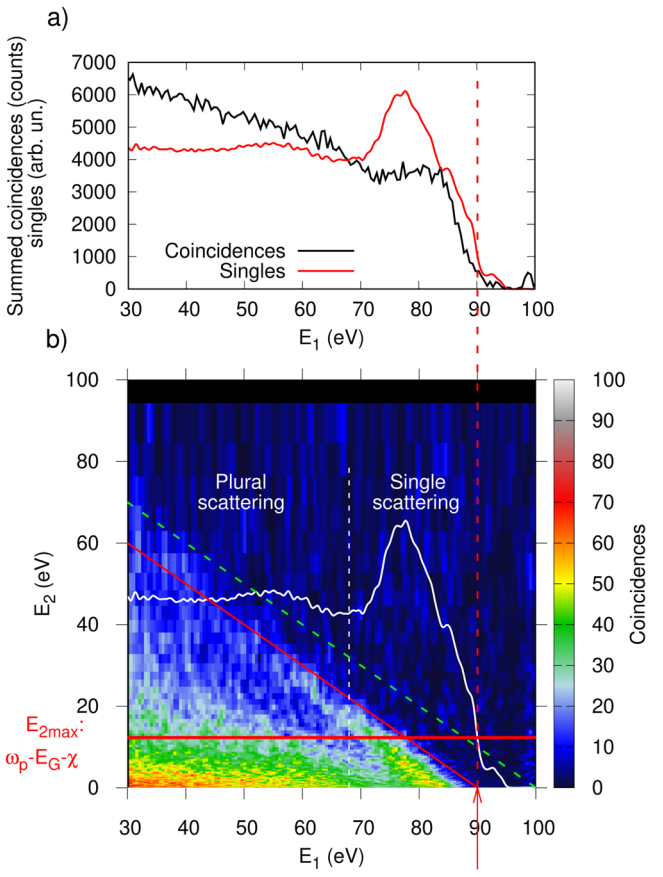


**Fig. 7.** (a) Comparison of the (singles) reflection electron energy loss spectrum (REELS, red curve) with the e2e-coincidence spectrum for arbitrary energies of the second electron $E_2$; (b) the (e,2e) double differential coincidence spectrum of $SiO_2$ overlayed with the REELS spectrum. The arrow denotes the onset of coincidences or the emission of the least bound electrons from the top of the valence band. The solid red line indicates the zero binding energy and the dashed green line corresponds to $E_1 + E_2 = E_0$.

scattered electron is transferred to a single solid-state electron which escapes as a secondary electron. If the energy would be transferred to more than one electron, no reasonable energy sharing model would be able to explain a rather sharp peak along the binding energy scale (or energy sum scale $E_1 + E_2$, see Eq. (1)), such as seen in the single scattering feature. Similar observations have earlier been published for Al [27–29] as well as for Ag and Si [30].

Furthermore, for larger energy losses $\Delta E > 30$ eV, i.e. in the multiple scattering range the number of coincidences is seen to increase with increasing energy loss in Fig. 7a, while the energies of the ejected electron (seen in Fig. 7b) correspond to the plasmon energy $\omega_p$ minus the height of the surface potential barrier, as per Eq. (1). This implies that multiple plasmon excitation predominantly proceeds via a Markov-type process [28], i.e. excitation of a double plasmon is incoherent and consists of successive excitation of single plasmons along the trajectory of an electron each of which decays via emission of a single electron with $E_2 = \omega_p - U_i$. This is in contrast to coherent double plasmon excitation and decay, where a double plasmon would be coherently excited in a single inelastic collision and – provided the entire energy loss would again be transferred to a *single* escaping electron – this would give rise to intensity in the (e,2e)-spectrum just below the red diagonal also for energy losses $\Delta E > 30$ eV, in extension of the single scattering feature.

In Fig. 8, the onset of the DIIMFP (shown in Fig. 5 is compared with the onset of coincidences (black curve in Fig. 7a). The numerical values of the onsets of the DIIMFP and the coincidence yield were determined

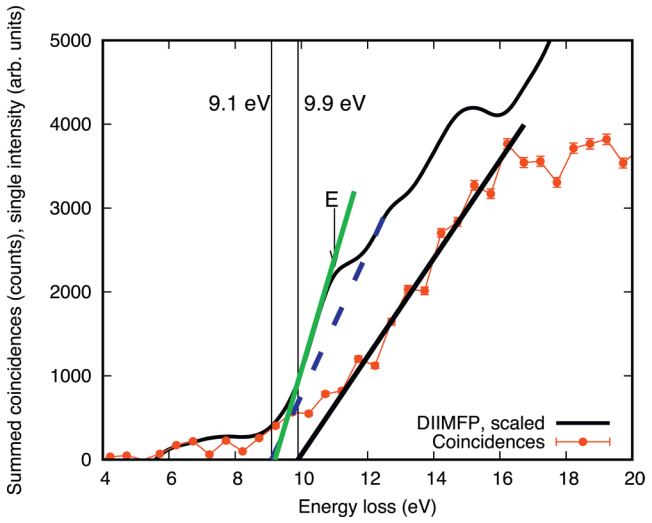


**Fig. 8.** The coincidence yield summed over $E_2$ (secondary electrons) compared with the DIIMFP. The onsets of the spectra were determined by doing a linear fit of the lowest energy loss feature, disregarding (blue dashed line) and including (green solid line) the exciton at 10.6 eV.

by a linear fit of the ridge representing the lowest energy loss. Since the band gap is assumed to be a bulk property, the onset of the DIIMFP rather than the loss spectrum is used to determine the band gap value of 9.1 eV (the values are in the range of 8–9 eV in the literature [31,32]). Note, that the inclusion or exclusion of the excitonic loss feature does not influence the determination of the band gap (see Fig. 8).

Using this procedure allows one to disregard the surface defect states and determine the value of the band gap more accurately. As discussed previously, the onset of the coincidences correspond to the height of the surface barrier of the material. The electron affinity $\chi$ then can be retrieved by using Eq. (3) (taking the difference between the onsets of the DIIMFP and the coincidence spectrum). The retrieved value of 0.8 eV agrees with the results found in the literature of 0.75 eV [33], 0.9 eV [34]. It has to be noted that the fitting procedure, used for the determination of the onsets produces a rather large error, which may exceed 100% in the value of $\chi$.

## 6. Conclusions

It has been shown that by taking two reflection electron energy loss (REELS) spectra, applying deconvolution algorithms [13,14] and the bivariate reversal method [11] it is possible to determine the optical constants and to distinguish the loss features associated with the presence of defects on the $SiO_2$ surface. The band gap determined from the differential inverse inelastic mean free path (DIIMFP) was 9.1 eV and is in a good agreement with values found in the literature [31,32]. The inelastic mean free path (IMFP) has been determined using the retrieved optical constants by using the Penn [23] and the Mermin [24] models and integration of the DIIMFP and is in a reasonable agreement (10 percent maximal deviation) with the TPP-2M formula [25]. The existence of plasmon is evidenced by the zero in the real part of the dielectric function at $\omega \approx 21$ eV. The coincidence measurements showed that the energy loss experienced by the scattered electron is transferred to a single solid-state electron mainly through plasmon decay. A Markov-type [28] successive excitation of single plasmons is seen from the multiple scattering region of the coincidence spectrum. By taking the difference of the onsets of coincidence spectrum and the DIIMFP the electron affinity has been determined to be 0.8 eV.

## Acknowledgments

Financial support by the FP7 People: Marie-Curie Actions Initial Training Network (ITN) SIMDALEE2 (Grant No. PITN 606988) is gratefully acknowledged.

## References

[1] H. Winter, J. Burgdörfer, Slow Heavy-Particle Induced Electron Emission from Solid Surfaces, Vol. 225 of Springer Tracts in Modern Physics, Springer, Vienna, 2007.
[2] J. Wiza, Microchannel plate detectors, Nucl. Instrum. Methods 162 (1979) 587, https://doi.org/10.1016/0029-554X(79)90734-1.
[3] J. Wiza, Sensors, Optical Sensors, John Wiley & Sons, 2008.
[4] T.J. Vink, A.R. Balkenende, R.G.F.A. Verbeek, H.A.M. van Hal, S.T. de Zwart, Materials with a high secondary-electron yield for use in plasma displays, Appl. Phys. Lett. 80 (12) (2002) 2216–2218, https://doi.org/10.1063/1.1464229.
[5] H.S. Uhm, E.H. Choi, G.S. Cho, Influence of secondary electron emission on breakdown voltage in a plasma display panel, Appl. Phys. Lett. 78 (5) (2001) 592–594, https://doi.org/10.1063/1.1343492.
[6] W.S. Werner, W. Smekal, C. Tomastik, H. Stri, Surface excitation probability of medium energy electrons in metals and semiconductors, Surf. Sci. 486 (3) (2001) L461–L466, https://doi.org/10.1016/S0039-6028(01)01091-3 URL: http://www.sciencedirect.com/science/article/pii/S0039602801010913.
[7] C. Tomastik, Determination of the inelastic mean free path of medium energy electrons in 24 elemental solids by means of elastic peak electron spectroscopy, Ph.D. thesis, Vienna University of Technology, 2004.
[8] S. Samarin, O. Artamonov, A. Suvorova, A. Sergeant, J. Williams, Measurements of insulator band parameters using combination of single-electron and two-electron spectroscopy, Solid State Commun. 129 (6) (2004) 389–393, https://doi.org/10.1016/j.ssc.2003.11.008 URL: http://www.sciencedirect.com/science/article/pii/S003810980300975X.
[9] M. Vos, S.W. King, B.L. French, Measurement of the band gap by reflection electron energy loss spectroscopy, J. Electron Spectrosc. Relat. Phenom. 212 (2016) 74–80, https://doi.org/10.1016/j.elspec.2016.08.001 URL: https://www.sciencedirect.com/science/article/pii/S0368204816300925.
[10] M. Vos, S.W. King, B.L. French, Measurement of the band gap by reflection electron energy loss spectroscopy, J. Electron Spectrosc. Relat. Phenom. 212 (2016) 74–80, https://doi.org/10.1016/j.elspec.2016.08.001 URL: https://www.sciencedirect.com/science/article/pii/S0368204816300925.
[11] W.S. Werner, Simple algorithm for quantitative analysis of reflection electron energy loss spectra (reels), Surf. Sci. 604 (3) (2010) 290–299, https://doi.org/10.1016/j.susc.2009.11.019 URL: http://www.sciencedirect.com/science/article/pii/S003960280900733X.
[12] W.S.M. Werner, Differential surface and volume excitation probability of medium-energy electrons in solids, Phys. Rev. B 74 (2006) 075421, https://doi.org/10.1103/PhysRevB.74.075421.
[13] S. Tougaard, I. Chorkendorff, Differential inelastic electron scattering cross sections from experimental reflection electron-energy-loss spectra: Application to background removal in electron spectroscopy, Phys. Rev. B 35 (1987) 6570–6577, https://doi.org/10.1103/PhysRevB.35.6570.
[14] H. Stefan, G. Alexander, W. Werner, Richardson–Lucy Deconvolution of reflection electron energy loss spectra, Surf. Interface Anal. 41 (5) (2009) 357–360 arXiv:https://onlinelibrary.wiley.com/doi/pdf/10.1002/sia.3006, doi:10.1002/sia.3006. URL https://onlinelibrary.wiley.com/doi/abs/10.1002/sia.3006.
[15] E.D. Palik, Handbook of Optical Constants of Solids Vol. 1 Academic, 1985.
[16] F. Bart, M. Gautier, F. Jollet, J. Duraud, Electronic structure of the (0001) and (1010) quartz surfaces and of their defects as observed by reflection electron energy loss spectroscopy (reels), Surf. Sci. 306 (3) (1994) 342–358, https://doi.org/10.1016/0039-6028(94)90076-0 URL: http://www.sciencedirect.com/science/article/pii/0039602894900760.
[17] D.L. Griscom, Defect structure of glasses: some outstanding questions in regard to vitreous silica, J. Non-Crystal. Solids 73 (1) (1985) 51–77, https://doi.org/10.1016/0022-3093(85)90337-0 Glass Science and Technology Problems and Prospects for 2004, http://www.sciencedirect.com/science/article/pii/0022309385903370.
[18] Y.-n. Xu, W.Y. Ching, Electronic and optical properties of all polymorphic forms of silicon dioxide, Phys. Rev. B 44 (1991) 11048–11059, https://doi.org/10.1103/PhysRevB.44.11048.
[19] L. Garvie, P. Rez, J. Alvarez, P. Buseck, Interband transitions of crystalline and amorphous SiO2: an electron energy-loss spectroscopy (EELS) study of the low-loss region, Solid State Commun. 106 (5) (1998) 303–307, https://doi.org/10.1016/S0038-1098(98)00021-0 URL: http://www.sciencedirect.com/science/article/pii/S0038109898000210.
[20] C. Kwei, Y. Chen, C. Tung, J. Wang, Electron inelastic mean free paths for plasmon excitations and interband transitions, Surf. Sci. 293 (3) (1993) 202–210, https://doi.org/10.1016/0039-6028(93)90314-A URL: http://www.sciencedirect.com/science/article/pii/003960289390314A.
[21] Y.F. Chen, C.M. Kwei, C.J. Tung, Optical-constants model for semiconductors and insulators, Phys. Rev. B 48 (1993) 4373–4379, https://doi.org/10.1103/PhysRevB.48.4373.
[22] S.G. Johnson, Nlopt version 2.4.2, (2014) https://nlopt.readthedocs.io/en/latest/.
[23] D.R. Penn, Electron mean-free-path calculations using a model dielectric function, Phys. Rev. B 35 (1987) 482–486, https://doi.org/10.1103/PhysRevB.35.482.
[24] N.D. Mermin, Lindhard dielectric function in the relaxation-time approximation, Phys. Rev. B 1 (5) (1970) 2362–2363, https://doi.org/10.1103/PhysRevB.1.2362.
[25] S. Tanuma, C.J. Powell, D.R. Penn, Calculations of electron inelastic mean free paths for 31 materials, Surf. Interface Anal. 11 (11) (1988) 577–589.

[26] R.A. Ferrell, J.J. Quinn, Characteristic energy loss of electrons passing through metal foils: momentum-exciton model of plasma oscillations, Phys. Rev. 108 (1957) 570–575.
[27] W.S.M. Werner, W. Smekal, H. Winter, A. Ruocco, F. Offi, S. Iacobucci, G. Stefani, Role of surface and bulk plasmon decay in secondary electron emission, Phys. Rev. B78 (2008) 233403.
[28] W.S.M. Werner, F. Salvat-Pujol, W. Smekal, R. Khalid, F. Aumayr, H. Störi, A. Ruocco, F. Offi, G. Stefani, S. Iacobucci, Contribution of surface plasmon decay to secondary electron emission from an Al surface, Appl. Phys. Lett. 99 (2011) 184102.
[29] W.S.M. Werner, F. Salvat-Pujol, A. Bellissimo, R. Khalid, W. Smekal, M. Novak, A. Ruocco, G. Stefani, Secondary-electron emission induced by in vacuo surface excitations near a polycrystalline al surface, Phys. Rev. B88 (2013) 201407.
[30] R. Khalid, F. Salvat-Pujol, W.S.M. Werner, Secondary electron energy loss coincidence (e,2e) spectroscopy on Ag and Si surfaces, J. Phys.: Conf. Ser. 439 (2013) 012003, https://doi.org/10.1088/1742-6596/439/1/012003.
[31] S.S. Nekrashevich, V.A. Gritsenko, Electronic structure of silicon dioxide (a review), Phys. Solid State 56 (2) (2014) 207–222, https://doi.org/10.1134/S106378341402022X.
[32] E. Vella, F. Messina, M. Cannas, R. Boscaino, Unraveling exciton dynamics in amorphous silicon dioxide: Interpretation of the optical features from 8 to 11 eV, Phys. Rev. B 83 (2011) 174201, https://doi.org/10.1103/PhysRevB.83.174201.
[33] V.W. Ballarotto, M. Breban, K. Siegrist, R.J. Phaneuf, E.D. Williams, Photoelectron emission microscopy of ultrathin oxide covered devices, J. Vacuum Sci. Technol. B 20 (6) (2002) 2514–2518, https://doi.org/10.1116/1.1525007 URL: http://scitation.aip.org/content/avs/journal/jvstb/20/6/10.1116/1.1525007.
[34] N. Fujimura, et al., Evaluation of valence band top and electron affinity of SiO 2 and Si-based semiconductors using S-ray photoelectron spectroscopy, Japan. J. Appl. Phys. 55 (8S2) (2016) 08PC06 URL: http://stacks.iop.org/1347-4065/55/i=8S2/a=08PC06.